Chapter 1
Solid Solution

1.1 Solubility

Hydrogen that causes deterioration of mechanical properties of metallic materials comes from environments during fabrication and service. Hydrogen adsorbs on the surface of metals as H_2 molecules or H_3O^+ ions, dissociates to atoms, and diffuses into the bulk. The hydrogen content depends on the type of the material, its internal and surface states, and environmental conditions such as temperature, humidity, and the presence of corrosive species. Hydrogen atoms locate in metals at various sites with respective energies, as schematically shown in Fig. 1.1. The role of hydrogen in embrittlement is the central subject of this book, and hydrogen interactions with lattice defects are crucial.

Hydrogen atoms in solid solution, i.e., at interstitial sites of the regular crystalline lattice, are intrinsic to a metallic material but are only a part of the total number of hydrogen atoms in most cases at thermal equilibrium. However, interstitial sites are dominant for the number and control of the transport and partition of hydrogen at various trap sites.

Solid solubility—the atomic fraction of hydrogen in the lattice at thermal equilibrium—is a function of temperature and hydrogen environments. Figure 1.2 [1] compares the temperature dependence of the solid solubility θ of hydrogen in various metals in hydrogen gas of 0.1 MPa. Both positive and negative dependencies on temperature are present in metals. The negative slope in the Arrhenius plot for iron means an endothermic reaction for hydrogen absorption, i.e., the hydrogen energy in the solid solution is higher than that in the hydrogen molecule, as Fig. 1.1 indicates. It contrasts with Ti and V, of higher affinities with hydrogen than Fe. The amount of absorbed hydrogen in iron at high temperatures is readily measurable by chemical analysis. The solid solubility data thus determined for pure iron under hydrogen gas environments above 573 K are shown in Fig. 1.3 [2]. The ordinate denotes θ in atomic ratio normalized by $\sqrt{p}$, where p is the hydrogen gas pressure in the unit of 0.1 MPa. Solubility data for iron at lower temperatures are in Sect. 2.1 concerning trapping of hydrogen in lattice defects.

M. Nagumo, *Fundamentals of Hydrogen Embrittlement*,
https://doi.org/10.1007/978-981-99-0992-6_1

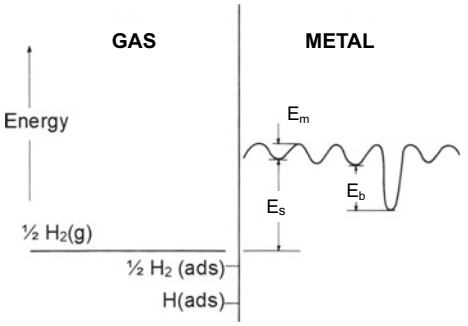

Fig. 1.1 Energies of hydrogen in gas-metal equilibria. E_s Energy of solid solution. E_m Migration energy. E_b Trap binding energy

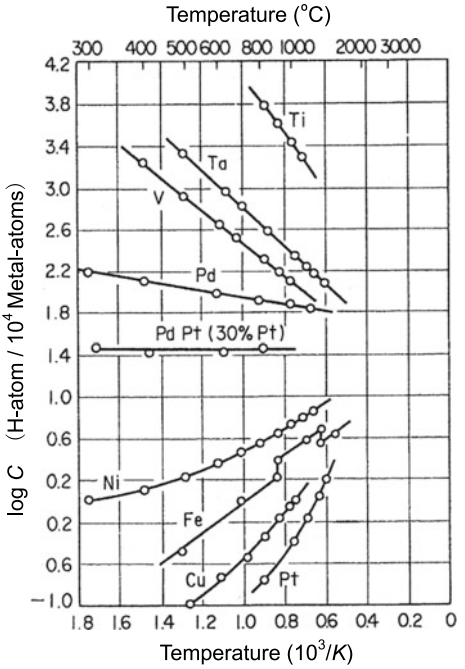

Fig. 1.2 Temperature dependence of hydrogen solubility in various metals in equilibrium at 0.1 MPa hydrogen gas (Huang et al. [1]. Reprinted with permission from The Japan Inst. Metals)

In Fig. 1.3, the level of θ in face-centered cubic (fcc) γ-iron is higher than that in body-centered cubic (bcc) α-iron, and a slight departure from linearity in the Arrhenius plot, i.e., the log C versus $1/T$ relation, appears at temperatures lower than about 773 K. The departure was discussed to originate in simultaneous occupations of tetrahedral and octahedral sites in α-iron [2]. Definitive values of θ in α-iron in the room temperature regime are few. Hirth collected reliable data and gave a useful expression of θ (in atomic ratio) in hydrogen gas of pressure p (in 0.1 MPa) in the form

$$\theta = 0.00185\sqrt{p}\exp(-3440/T) \tag{1.1}$$

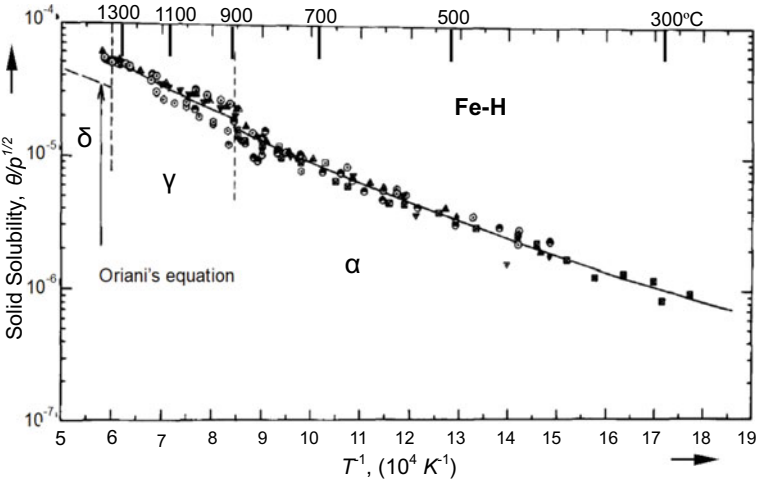

Fig. 1.3 Solid solubility of hydrogen in iron above 573 K (Different marks are by literatures in the original paper) (Da Silva et al. [2])

with T in Kelvin [3]. The heat of solution of hydrogen in α-iron obtained from the temperature dependence of θ is 28.6 kJ/mol-H.

The $\sqrt{p}$ dependence of θ is known as Sieverts' law. It is originally an experimental relation for diatomic molecular gases, but thermodynamics also derives the law in the following way. The entry of hydrogen into metal starts from the dissociation of adsorbed hydrogen molecules on the metal surface, followed by the diffusion of hydrogen atoms into the metal. For the equilibrium reaction

$$\frac{1}{2}\mathrm{H}_2 \rightleftarrows \mathrm{H}_{\mathrm{sol}}, \tag{1.2}$$

where the chemical potential μ is equal in both sides, i.e.

$$\frac{1}{2}\mu_{\mathrm{H}_2} = \mu_{\mathrm{H}_{\mathrm{sol}}}. \tag{1.3}$$

The expression of μ using its value at the standard state, μ^0, and the hydrogen concentration in terms of the activity, a, is

$$\mu = \mu^0 + RT \ \ln \ a, \tag{1.4}$$

where R is the gas constant. By definition of μ, the change of the Gibbs energy associated with the absorption of hydrogen is

$$-\Delta G^0 = \frac{1}{2}\mu^0_{\mathrm{H}_2} - \mu^0_{\mathrm{H}_{\mathrm{sol}}} = RT \ \ln \ \frac{a_{\mathrm{H}_{\mathrm{sol}}}}{a^{1/2}_{\mathrm{H}_2}}. \tag{1.5}$$

Since

$$\Delta G^0 = \Delta \mathrm{H}^0 - T\Delta \mathrm{S}^0, \tag{1.6}$$

where H and S denote respectively enthalpy and entropy, Eq. (1.5) is rewritten as

$$a_{\mathrm{H_{sol}}} = a_{\mathrm{H_2}}^{1/2} \exp\left(-\frac{\Delta \mathrm{H}^0}{RT}\right) \exp\left(\frac{\Delta \mathrm{S}^0}{R}\right), \tag{1.7}$$

leading to the form of Sieverts' law.

An increase in the hydrogen partial pressure augments the hydrogen concentration. The associated change in the volume differs between ideal and real gases, and the change in the chemical potential in a real gas is expressed by defining and introducing fugacity f instead of pressure p in an ideal gas, i.e.,

$$\mathrm{d}\mu = RT\ \mathrm{d}\ln f. \tag{1.8}$$

From Eqs. (1.8) and (1.4), an expression of the hydrogen activity a in terms of fugacity f is

$$a = \frac{f}{f^0} = \frac{\varphi p}{\varphi^0 p^0}, \tag{1.9}$$

where φ is the fugacity coefficient and the superscript "^{0}" denotes the standard state.

Accordingly, for estimating the equilibrium hydrogen concentration using Eq. (1.1), p should be replaced by f. The conversion is necessary for practice in high pressures since φ increases with p. Calculated values of φ are tabulated in Ref. [4], e.g., 1.06, 1.41, and 2.06 for p of 10, 50, and 100 MPa hydrogen gas at 300 K, but the values vary according to the equation of state employed for the calculation. The equilibrium hydrogen concentration in α-iron at room temperature expected from Eq. (1.1) is minimal, *ca* 2×10^{-8} (in atomic ratio), in 0.1 MPa hydrogen gas. Then, usually observed hydrogen concentrations of the order of mass ppm in ferritic steels are mostly of trapped hydrogen in various lattice defects except under non-equilibrium situations.

The solubility of hydrogen in steel is substantially altered by alloying. In austenitic stainless steels, the heat of solution of hydrogen is about 16 kJ/mol-H [5], much less than that in pure γ-iron. Solubility data for stainless steels are shown in Fig. 1.4 [5]. Higher solubilities in austenitic stainless steels than those in ferritic stainless steels are due not only to the crystal structures but also to alloying elements such as Ni and Cr. Most data in Fig. 1.4 are by permeation experiments. It is to be noticed that the distributions of hydrogen in austenitic stainless steel are often very inhomogeneous because of the low diffusivity of hydrogen, as described in Sect. 4.1.1. At elevated temperatures, the increased diffusivity favors homogeneous distribution, and the hydrogen content in Type 316L stainless steel directly measured using thermal desorption is about 40 mass ppm in 70 MPa hydrogen at 363 K [6].

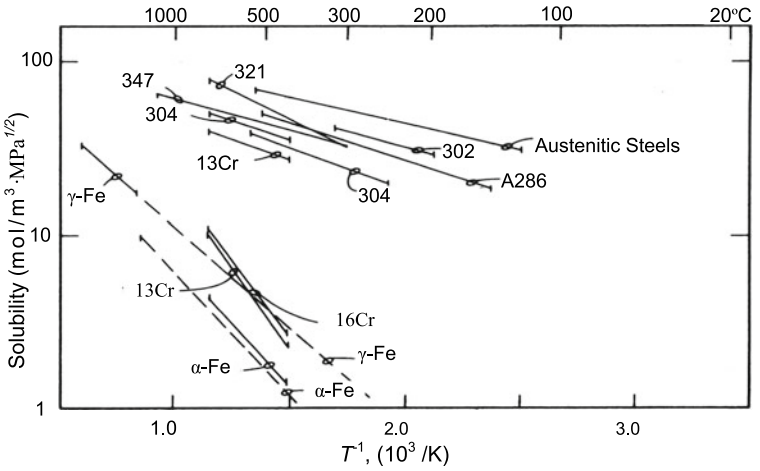

Fig. 1.4 Solid solubility data of hydrogen in stainless steel (Caskey [5])

1.2 Lattice Location

Hydrogen atoms locate at interstitial sites in the elementary lattice of α-iron. Direct determination of the location is difficult because of the hydrogen's low solubility and high diffusivity. However, calculations of the total energy of the solution, described in Sect. 1.4, showed preferential occupancy at the tetragonal site (T-site) than at the octahedral site (O-site). Analyses of thermodynamic data also showed a favored occupancy at the T-site at low temperatures, while the O-site occupancy increased with the temperature rise [2, 7].

A powerful method to directly detect the lattice location of hydrogen in metals is a channeling analysis utilizing a nuclear reaction ^{1}H(^{11}B, α)$\alpha\alpha$ using ^{11}B beam. The location of hydrogen can be precisely determined by measuring the angular profile of emitted α particles on tilting a single crystal specimen against the incident ^{11}B beam. Hydrogen occupancy at the T-site was successfully confirmed for bcc single crystals of the group V_a metals (Nb, V, Ta) and their alloys [8–11]. In vanadium, a reversible displacement of hydrogen from the normal T-site occurred when compressive stress of 70 MPa was applied along the <100> axis [8]. In Nb-Mo alloys with Mo of less than 10%, the position of the hydrogen atom shifts from the center of the T-site to a neighboring Mo atom, as shown schematically in Fig. 1.5 [10]. The shift decreases with increasing Mo concentrations and disappears at 20 at.% of Mo, directly showing hydrogen trapping by alloying elements.

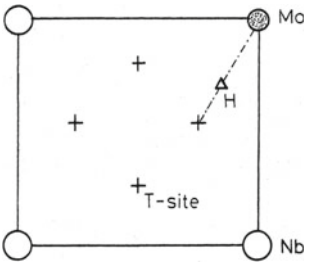

Fig. 1.5 Location of hydrogen atom in Nb–Mo alloy determined by a $^{1}H(^{11}B\alpha)\alpha\alpha$ nuclear reaction channeling method (Yagi [10]. Reprinted with permission from The Iron and Steel Institute Japan)

1.3 Partial Molar Volume and Strain Field

The entry of hydrogen into metals accompanies volume expansion, and dilatation measurements are available for direct determination of the partial molar volume of hydrogen, $\overline{V}_H$. While a substantial scatter of data is inevitable, a reliable $\overline{V}_H$ value for α-iron wires exposed to hydrogen gas is 2.0×10^{-6} m^3/mol-H in the temperature range from 873 to 1073 K [12]. Electrochemical hydrogen permeation experiments are alternative methods for determining $\overline{V}_H$ at room temperature. The applied elastic stress affects the steady-state permeation current in iron due to the change in the hydrogen solubility. The chemical potential of hydrogen in metal alters by the applied stress, and an additional hydrogen flow occurs to keep equilibrium. The hydrogen concentration evaluated from the permeation-current density gives $\overline{V}_H$ as [13],

$$\overline{V}_H = RT\left[\frac{\partial \ \ln\left(C_\sigma / C_0\right)}{\partial \ \sigma_h}\right], \tag{1.10}$$

where C_σ and C_0 are respectively hydrogen concentrations with and without the application of external hydrostatic stress σ_h.

A method to evaluate C_σ and C_0 is to measure reversible permeation current densities on cyclic stressing, and the obtained $\overline{V}_H$ for pure iron and AISI 4340 steel are 2.66×10^{-6} and 1.96×10^{-6} m^3/mol-H, respectively [13], which are close to the value obtained from dilatation measurements at high temperatures. The value of $\overline{V}_H$ is insensitive to temperature and microstructures. The value of 2.0×10^{-6} m^3/mol-H, i.e., about 0.3 nm^3/H-atom, is almost common for all metals [7]. However, Hirth noticed [3] that the value of $\overline{V}_H$ included an effect associated with elastic relaxation at the free surface and that the internal volume change δv for calculating interactions with the hydrostatic elastic fields of lattice defects was 1.22×10^{-6} m^3/mol-H.

The volume change around the hydrogen atom is crucial in the interaction energies of hydrogen with various types of lattice defects, described in Chap. 3. In α-iron, the local strain field around a single hydrogen interstitial atom has tetragonal symmetry in both the *T*- and *O*-sites [3], but the tetragonality is considered small. Accordingly, in the elastic regime, the hydrogen concentration, C_h, under hydrostatic stress σ_h, or C_σ under a uniaxial stress σ, at a constant hydrogen fugacity f is given respectively as

$$C_h = C_0 \exp\left(\frac{\sigma_h \overline{V}_H}{RT}\right)_f, \tag{1.11}$$

or

$$C_\sigma = C_0 \exp\left(\frac{\sigma \overline{V}_H}{3RT}\right)_f, \tag{1.12}$$

where C_0 is the value at zero stress [14].

Stress fields in materials are generally inhomogeneous and result in localized hydrogen distributions. An example is the hydrogen accumulation in stress-concentrated areas such as notch root [15]. Visualizing hydrogen distributions is described in Sect. 2.3. It should be careful that the local increase in the hydrogen concentration by stress is not only for hydrogen in solid solution but also for hydrogen trapped in various lattice defects created by plastic strain. In embrittlement, generation and activation of lattice defects deteriorate materials, and the crucial role of strain-induced defects, rather than hydrogen itself, is described in later chapters.

1.4 Atomistic Calculations of the Heat of Solution

In the crystalline lattice of metals, the electronic state of hydrogen differs from that of a free atom because of the partial sharing of electrons with host metallic ions. The heat of solution, *Hs*, is the difference between the energy of hydrogen atom in solid solution and half of the energy of hydrogen molecule as shown in Fig. 1.1. Atomistic calculations of binding energies of hydrogen with metals have been conducted by various methods. The first-principles calculations are generally time-consuming, and some approximate methods have been devised.

The effective medium theory (EMT) replaces the complicated inhomogeneous host with an effective host consisting of a homogeneous electron gas. The embedding energy ΔE of an atom is the energy difference between the combined atom–host system minus the energies of the separated atom and the host. The host density is not homogeneous in general, and the core regions of host atoms have substantial variations in the electrostatic potential. Nørskov took into account the interaction of the hydrogen 1*s* level with the valence bands, mainly 3*d* band, of the host and calculated ΔE of hydrogen at the *T*-site of α-iron in transition metals [16]. The calculated value of ΔE for α-iron was -212 kJ/mol. The heat of solution is the embedding energy minus the binding energy of a hydrogen molecule (−232 kJ/mol), and the resultant 20 kJ/mol is about two-thirds of the experimentally obtained heat of solution of 29 kJ/mol [3, 17].

A generalization of the EMT using a pair-wise interaction is the embedded atom method (EAM) [18, 19]. It considers each atom in a system as embedded in a host

lattice consisting of all other atoms. An employed approximation is that the embedding energy depends only on the environment immediately around the impurity or locally uniform electron density. The energy of an impurity atom in a host consists of two terms; one is a function of the electron density of the host without impurity, and the other is the short-range electrostatic interaction. The total energy is a sum of all individual contributions of the host and the impurity. Daw and Baskes determined the embedding energies semiempirically and calculated the adsorption energies on the surfaces of Pd and Ni. Agreements with experimental values were fairly good for Pd, but calculated values were much smaller than experiments for Ni. For the bcc iron–hydrogen system, Wen et al. proposed a new potential to use in the EAM calculation [20]. Using empirically determined parameters for fitting, Wen et al. obtained good agreements between calculated and experimental values for the heat of solution, migration energy, and hydrogen binding energy with vacancies.

On the other hand, Itsumi and Elis calculated electronic structures for bcc iron clusters with or without hydrogen and also involving a vacancy [21]. The calculations used local-density functional theory, implemented by the Discrete Variational Method (DV-Xα). Calculations of the density of states for α-Fe clusters of 32 atoms with and without one hydrogen atom showed that the main bonding peak was due to H-1 *s* and Fe-4 *s* hybridization with smaller contributions of Fe-3*d* and 4*p*. The charge transfer of about 0.6*e* from the first and second neighbor Fe atoms to H decreased metallic bond strength. Itsumi and Elis used the concept of the bond orders, defined as the sum of overlap populations between two atoms, as a measure of interatomic bonding strength. Interstitial hydrogen notably decreases Fe–Fe bond strength, but the acting area is over a small distance within 0.3 nm. The Fe–H bond strength increases by nearby vacancies associated with a shift of the position of the hydrogen atom toward the vacancy.

The total energy of the many-electron system at the ground state is a function of the spatially dependent electron density. Tateyama et al. applied the density functional theory (DFT) to calculate the total energy of the H–α–Fe system using a pseudopotential and a plane-wave basis set [22]. A supercell consisting of 54 atoms (53 Fe-atoms + 1 H-atom) was adopted, locating hydrogen at a *T*-site as the ground state. The calculated heat of solution was 32.8 kJ/mol-H, which corresponded to an experimentally determined value of 29 kJ/mol-H. Effects of the supercell size or applied pressure on the system's total energy were also calculated [23]. The calculated heat of solution was a decreasing function of hydrostatic tensile stress that increased cell volume, a natural consequence of the repulsive nature of the solid solution. It was deduced that the hydrogen concentration in a stress-concentrated region, e.g., ahead of a crack tip, increases about 100-fold when applied hydrostatic tensile stress of 2–5 GPa.

Another calculation of the heat of solution using DFT with different computational supercell sizes, i.e., different hydrogen concentrations, showed the heat of solution of 28.9 kJ/mol in the *T*-site of α-iron [24]. The energy difference between hydrogen in the *O*-site and *T*-site converged as the hydrogen concentration decreased, suggesting the operation of a repulsive interaction between hydrogen atoms.

Calculations of the formation energy of a Fe–H complex using DFT were also conducted with a supercell of 54 Fe atoms [25]. The formation energy was defined, similarly to the embedding energy, as the energy of the complex minus the total energy of Fe atoms in a cell and the energy of one hydrogen atom in the isolated hydrogen molecule. The calculated formation energies for the *T*-site and *O*-site occupancy were 20.3 and 32.8 kJ/mol, respectively. The value of 20.3 kJ/mol corresponds to 20 J/mol obtained by the EMT method [16] but differs from the experimental heat of solution of around 28.6 kJ/mol. Counts et al. ascribed the gap to the zero-point-energy of the lattice vibration for hydrogen in α-iron and corrected the value to 28.9 kJ/mol in agreement with the experimental one [25].

References

1. Y.G. Huang, K. Fujita, H. Uchida, Bull. Jpn. Inst. Metals **18**, 694–703 (1979)
2. J.R.G. da Silva, S.W. Stafford, R.B. McLellan, J. Less Common Metals **49**, 407–420 (1976)
3. J.P. Hirth, Metall. Trans. A **11A**, 861–890 (1980)
4. H P. van Leeuwen, in *Hydrogen Degradation of Ferrous Alloys*, eds. by R.A. Oriani, J.P. Hirth, M. Smialowski (Noyes Pub., Park Ridge N.J. 1985), pp. 16–35
5. G.R. Caskey, Jr., in *Hydrogen Degradation of Ferrous Alloys*, eds. by R.A. Oriani, J.P. Hirth, M. Smialowski (Noyes Pub., Park Ridge N.J., 1985), pp. 822–862
6. K. Takai, K. Murakami, N. Yabe, H. Suzuki, Y. Hagiwara, J. Jpn. Inst. Metals **72**, 448–456 (2008)
7. K. Kiuchi, R.B. McLellan, Acta Metall. **31**, 961–984 (1983)
8. Y. Yagi, T. Kobayashi, S. Nakamura, F. Kano, K. Watanabe, Y. Fukai, S. Koike, Phys. Rev. B **33**, 5121–5123 (1986)
9. Y. Yagi, T. Kobayashi, Y. Fukai, K. Watanabe, J. Phys. Soc. Jpn. **52**, 3441–3447 (1983)
10. E. Yagi, ISIJ Int. **43**, 505–513 (2003)
11. C. Sugi, E. Yagi, Y. Okada, S. Koike, T. Sugawara, T. Shishido, K. Ogiwara, J. Phys. Soc. Jpn. **82**, 074601 (2013)
12. H. Wagenblast, H.A. Wriedt, Metall. Trans. **2**, 1393–1397 (1971)
13. J. O'M Bockris, P.K. Subramanyan, Acta Metall. **19**, 1205–1208 (1971)
14. H.A. Wriedt, R.A. Oriani, Acta Metall. **18**, 753–760 (1970)
15. K. Ichitani, M. Kanno, S. Kuramoto, ISIJ Int. **43**, 496–504 (2003)
16. J.K. Nørskov, Phys. Rev. B **26**, 2875–2885 (1982)
17. W.J. Arnoult, R.B. McLellan, Acta Metall. **21**, 1396–1397 (1973)
18. M.S. Daw, M.I. Baskes, Phys. Rev. Lett. **50**, 1285–1288 (1983)
19. M.S. Daw, M.I. Baskes, Phys. Rev. B **29**, 6443–6453 (1984)
20. M. Wen, X.-J. Xu, S. Fukuyama, K. Yokogawa, J. Mater. Res. **16**, 3496–3502 (2001)
21. Y. Itsumi, D.E. Ellis, J. Mater. Res. **11**, 2206–2213 (1996)
22. Y. Tateyama, T. Miyazaki, T. Ohno, Phys. Rev. B, **67**, 174105-1-0 (2003)
23. Y. Tateyama, T. Ohno, ISIJ Int. **43**, 573–578 (2003)
24. D.E. Jiang, E.A. Carter, Phys. Rev. B **70**, 064102 (2004)
25. W.A. Counts, C. Wolverton, R. Gibala, Acta Mater. **58**, 4730–4741 (2010)